Pronounced loss of Amazon rainforest resilience since the early 2000s

Chris Boulton (C.A.Boulton@exeter.ac.uk)
University of Exeter https://orcid.org/0000-0001-7836-9391
Timothy Lenton
Univeristy of Exeter https://orcid.org/0000-0002-6725-7498
Niklas Boers
Potsdam Institute for Climate Impact Research https://orcid.org/0000-0002-1239-9034

Article

Keywords: global carbon cycle, climate change, biodiversity, carbon storage

Posted Date: April 14th, 2021

DOI: https://doi.org/10.21203/rs.3.rs-379902/v1

Version of Record: A version of this preprint was published at Nature Climate Change on March 7th, 2022.
See the published version at https://doi.org/10.1038/s41558-022-01287-8.

Pronounced loss of Amazon rainforest resilience since the early 2000s

Chris A. Boulton[1*], Timothy M. Lenton[1] & Niklas Boers[1,2,3,4]

[1]Global Systems Institute, University of Exeter, Exeter, UK.

[2]Department of Mathematics, University of Exeter, UK

[3]Department of Mathematics, Free University of Berlin, Germany

[4]Potsdam Institute for Climate Impact Research, Potsdam, Germany

*Corresponding author: c.a.boulton@exeter.ac.uk

The resilience of the Amazon rainforest to climate and land-use change is of critical importance for biodiversity, regional climate, and the global carbon cycle. Some models project future climate-driven Amazon rainforest dieback and transition to savanna[1]. Deforestation and climate change, via increasing dry-season length[2,3] and drought frequency – with three 1-in-100-year droughts since 2005[4-6] – may already have pushed the Amazon close to a critical threshold of rainforest dieback[7,8]. However, others argue that CO_2 fertilization should make the forest more resilient[9,10]. Here we quantify Amazon resilience by applying established indicators[11] to remotely-sensed vegetation data with focus on vegetation optical depth (1991-2016), which correlates well with broadleaf tree coverage. We find that the Amazon rainforest has been losing resilience since 2003, consistent with the approach to a critical transition. Resilience is being lost faster in regions with less rainfall, and in parts of the rainforest that are closer to human activity. Given observed increases in dry-season length[2,3] and drought frequency[4-6], and expanding areas of land use change, loss of resilience is likely to continue. We provide direct empirical evidence that the Amazon

rainforest is losing stability, risking dieback with profound implications for biodiversity, carbon storage and climate change at a global scale.

There is widespread concern about the resilience of the Amazon rainforest to land-use change and climate change. The Amazon is recognised as a potential tipping element in the Earth's climate system[12], is a crucible of biodiversity[13], and usually acts as a large terrestrial carbon sink[14]. The net ecosystem productivity (carbon uptake flux) of the Amazon has, however, been declining over the last four decades and during two major droughts in 2005 and 2010, the Amazon temporarily turned into a carbon source, due to increased tree mortality[15-17]. Several studies have suggested that deforestation[18] and anthropogenic global warming[1,5], especially in combination, could push the Amazon rainforest past critical thresholds[7,8] where positive feedbacks propel abrupt and substantial further forest loss. Two types of positive feedback are particularly important. First, localised fire feedbacks amplify drought and associated forest loss by destroying trees[19], and the fire regime itself may 'tip' from localised to 'mega-fires'[20]. Second, deforestation and forest degradation, whether due to direct human intervention or droughts, reduce evapotranspiration and hence the moisture transported further westward, reducing rainfall and forest viability there[21] and establishing a large-scale moisture recycling feedback. Net rainfall reduction may in turn reduce latent heating over the Amazon to the extent that it weakens the low-level circulation of the South American monsoon[18]. Model projections of future changes in the Amazon rainforest differ widely[1,9,10,22]. Early studies showed that the Amazon rainforest may exhibit strong dieback by the end of the 21st century[1,23]. Both pronounced drying in tropical South America and a weak CO_2 fertilisation effect[9] contributed to this result, with dieback also more common under stronger greenhouse gas emission scenarios[10]. Other studies based on varying general circulation and vegetation model components show a wider range of results[24,25]. Nevertheless, the forest may be 'committed' to dieback despite appearing stable at the end of model runs[26]. This highlights the importance of measuring the changing dynamical

stability of the forest alongside its mean state. Given the uncertainty in model projections, we directly analyse observational data for signs of resilience loss in the Amazon.

The mean state of a system is not usually informative of changes in resilience; either can change whilst the other remains constant. Thus, higher-order statistical characteristics that respond more sensitively to destabilisation than the mean need to be considered to quantify resilience. To measure the changing resilience of the Amazon rainforest, we use a stability indicator used to predict the approach of a dynamical system towards a bifurcation-induced critical transition. The predictability arises from the phenomenon of critical slowing down[27,28] (CSD): as the currently occupied equilibrium state of a system becomes less stable, it responds more sluggishly to short-term perturbations (e.g. weather variability for the Amazon). This loss of resilience (defined[29] as return rate from perturbation) reflects a weakening of negative feedbacks that maintain stability. The behaviour can be detected by an increase in lag-1 autocorrelation (AR(1)) in time series capturing the system dynamics[30,31]. It may also manifest as an increase in variance over time, but variance can also be easily influenced by changing variability of the perturbations driving the system[32]. Increasing AR(1) has been used to detect critical slowing down prior to bifurcation-induced state transitions in a number of systems, including but not limited to climate[30,33] and ecology[34]. A caveat, highlighted by analysis of model projections prior to Amazon dieback[32], is that a system should be forced slower than its intrinsic response timescale for CSD to occur (see Methods). Hence, the absence of CSD may not rule out the possibility of a forthcoming critical transition. Conversely, increasing AR(1) can sometimes occur for other physical reasons. A space-for-time substitution has previously revealed that tropical forest resilience as measured by mean AR(1) (on a grid point basis) is lower for less annual rainfall sums[11], but changes of Amazon resilience over time have not been investigated so far.

We investigate controls on the resilience of the Amazon vegetation system and how its resilience has changed over the last three decades, in terms of a changing AR(1) coefficient as estimated from satellite-derived vegetation data. The main dataset we use is from the

Vegetation Optical Depth Climate Archive (VODCA)[35], but we also analyse the NOAA Advanced Very-High-Resolution Radiometer's (AVHRR) normalized difference vegetation index NDVI[36] for comparison. Vegetation Optical Depth (VOD) has been previously used to estimate changes in vegetation biomass[37], whereas NDVI is more commonly used to measure the greenness of vegetation, i.e. photosynthetic activity[38]. We use the Ku-band product from VODCA, which has a resolution of 0.25°x0.25°, and for direct comparison we rescale the NDVI data to the same resolution. We focus on two stressors of the Amazon that may cause resilience changes – precipitation and human influence.

We use the Amazon basin as our study region and focus on those grid boxes which have a broadleaf fraction greater than or equal to 80% evergreen broadleaf (BL) fraction according to the MODIS Land Cover Type product in 2001[39] (See Methods). Figure 1 shows that when comparing BL fraction in 2001 to mean annual precipitation (MAP) from 2001-2016 (from CHIRPS[40]; see Methods), there is a clear bimodal region visible between approximately 1500-2250mm, which has been reported previously[41-43] (Fig.1a). Bi-stability, where a forested or non-forested area can exist under the same MAP, suggests the potential for bifurcation- and noise-induced transitions, the latter potentially triggered by single perturbations such as droughts or fires. Over most of the region, BL fraction has not changed significantly between 2001 and 2016 (Fig. 1b). However, deforestation has occurred along parts of the southern and eastern edges of the rainforest, along parts of the Amazon river, and in some northern parts of the basin.

With a very similar spatial pattern as the change in BL fraction (Fig. 1b), we find decreases in VOD around the south-eastern edges of the forest (Fig. 1c). Averaged across the Amazon study region we find overall decreasing VOD, which matches with the observed decrease in the number of grid boxes that have BL >= 80% each year (Fig. 1d). NDVI, in contrast, does not agree spatially with the changes in BL fraction – rather, NDVI increases in the south-eastern parts of the Amazon where deforestation rates are known to be high (Supplementary Fig. 1). Changes in BL fraction from 2001-2016 are strongly correlated with changes in VOD

over the same period (Fig. 1e), whereas changes in NDVI are not (Fig. 1f), echoing previous in-situ comparisons between VOD and NDVI[44]. Hence, we focus our analysis on VOD in the following, with results for NDVI in the Supplementary Figures.

We begin our resilience analysis by focusing on the temporal changes of AR(1), computed in sliding windows from the nonlinearly detrended and de-seasonalised VOD time series (see Fig. 2, and Methods). The time series calculated from the mean AR(1) value across our study area each month shows a substantial increase over time, particularly from ~2003 (Fig. 2a). The spatial distribution of the AR(1) tendency, measured by the Kendall rank correlation coefficient τ (see Methods) at each grid box, shows that decreases in AR(1) (increases in resilience) are mostly restricted to parts of the region with higher mean annual precipitation (MAP) (Fig. 2b). We also observe stable or decreasing AR(1) values around the tributaries of the Amazon river, where vegetation growth will be less dependent on precipitation for water availability. Overall, the majority (74.6%) of grid boxes show increasing AR(1) values and hence, loss of resilience (Fig. 2c). Using alternative methods of detrending the VOD time series (see Methods) yields similar results (Supplementary Fig. 2). A predominance of increasing AR(1) trends is also found for the NDVI time series since 2003 (Supplementary Fig. 3).

To further explore the relationship between MAP and AR(1) trend, we create mean AR(1) time series on a moving MAP-band of 500mm (see Methods). These bands show broadly the same behaviour as the region overall (Fig. 3a), with all bands showing a significant decrease in resilience post-2003 ($p<0.001$). The increase in AR(1) post-2003 appears least pronounced for the highest rainfall band (3500-4000mm). Sure enough, the intensity of resilience loss increases as the MAP-band decreases below 3500-4000mm (Fig. 3b). For NDVI, the same relationship is also observed (Supplementary Fig. 4a,b). However, due to a large decrease in NDVI AR(1) pre-2003 across the region, analysing the full AR(1) time series yield decreasing AR(1) Kendall τ coefficients for the higher MAP-bands.

It has previously been suggested that the forest near human land-use areas is less resilient[42]. To determine if this is shown by VOD, we measure the distance of each grid box from human land use in 2016 (see Methods, Supplementary Fig. 5). Calculating mean AR(1) time series on 50km distance bands, shows increases in AR(1) post-2003 are stronger for grid boxes closer to human land use (Fig. 4a). Grid boxes that are in more remote locations still show a loss of resilience but the AR(1) time series for these are more variable – likely because the area they are averaged over shrinks and becomes more disconnected (Fig. 4a). Above 200-250km away from human land use the signal of loss of resilience becomes less pronounced (Fig. 4b). NDVI time series also show there is a loss of resilience from 2003, in grid boxes that are closer than 200km from human land use (Supplementary Fig. 4c,d).

Our results suggest that the loss of resilience of the Amazon rainforest that is especially pronounced since 2003 (Fig. 2), could be due to a combination of changing precipitation patterns (Fig. 3) and changing human interference in the region (Fig. 4). Here we reason that as lower baseline MAP and greater proximity to human interference are both associated with greater loss of resilience, declining MAP and/or increasing human interference may be expected to cause increased resilience loss. We find increases in human land use areas using the MODIS Land Cover data over the time period, both in reach and intensity (Supplementary Fig. 6). However, although there are large parts of the study region with decreasing MAP, by comparing the spatial pattern of MAP decreases to the AR(1) increases (Supplementary Fig. 7), it is unlikely that the changes in MAP are the dominant driver of Amazon rainforest resilience loss. Rather, increases in dry-season length as reported in several recent studies[2,3,45,46] may explain the loss in vegetation resilience since the early 2000s detected here. With a longer study period to measure trends in MAP, it is possible that a stronger correlation between MAP changes and changes in resilience over time may be found.

The changes in forest resilience observed as increasing AR(1) in both vegetation indices are supported by another indicator of critical slowing down, namely increasing variance[33] – of both VOD (Supplementary Figure 8) and NDVI (Supplementary Figure 9). We note that variance is more strongly affected by changes in the frequency and amplitude of the forcing of a system, and as such results could be biased towards individual events. This, along with other issues, has led AR(1) to be considered a more robust indicator[47].

As emphasized above, changes in BL fraction do not directly relate to changes in resilience. Indeed, we infer a marked loss of resilience in terms of increasing AR(1) in vast areas where the BL fraction does not strongly decrease (compare Figs. 1b and 2b). One possible interpretation of this from model behaviour is that part of the Amazon rainforest might already be committed to dieback[26] despite not yet showing a strong change in mean state. Our results suggest that the overall loss of Amazon resilience we find since the early 2000s is attenuated in regions with higher rainfall and amplified in areas closer to human land use change. This suggests that reducing deforestation will not just protect the parts of the forest that are directly threatened but also benefit Amazon rainforest resilience over a much larger area.

References

1 Cox, P. M., Betts, R. A., Jones, C. D., Spall, S. A. & Totterdell, I. J. Acceleration of global warming due to carbon-cycle feedbacks in a coupled climate model. *Nature* **408**, 184-187, doi:10.1038/35041539 (2000).

2 Fu, R. *et al.* Increased dry-season length over southern Amazonia in recent decades and its implication for future climate projection. *Proceedings of the National Academy of Sciences* **110**, 18110-18115, doi:10.1073/pnas.1302584110 (2013).

3 Leite-Filho, A. T., Sousa Pontes, V. Y. & Costa, M. H. Effects of Deforestation on the Onset of the Rainy Season and the Duration of Dry Spells in Southern Amazonia. *Journal of Geophysical Research: Atmospheres* **124**, 5268-5281, doi:10.1029/2018jd029537 (2019).

4 Lewis, S. L., Brando, P. M., Phillips, O. L., Van Der Heijden, G. M. F. & Nepstad, D. The 2010 Amazon Drought. *Science* **331**, 554-554, doi:10.1126/science.1200807 (2011).

5 Cox, P. M. *et al.* Increasing risk of Amazonian drought due to decreasing aerosol pollution. **453**, 212-215, doi:10.1038/nature06960 (2008).

6 Erfanian, A., Wang, G. & Fomenko, L. Unprecedented drought over tropical South America in 2016: significantly under-predicted by tropical SST. *Scientific Reports* **7**, doi:10.1038/s41598-017-05373-2 (2017).

7 Lovejoy, T. E. & Nobre, C. Amazon Tipping Point. *Science Advances* **4**, eaat2340, doi:10.1126/sciadv.aat2340 (2018).

8 Lovejoy, T. E. & Nobre, C. Amazon tipping point: Last chance for action. *Science Advances* **5**, eaba2949, doi:10.1126/sciadv.aba2949 (2019).

9 Huntingford, C. *et al.* Simulated resilience of tropical rainforests to CO2-induced climate change. **6**, 268-273, doi:10.1038/ngeo1741 (2013).

10 Boulton, C. A., Booth, B. B. B. & Good, P. Exploring uncertainty of Amazon dieback in a perturbed parameter Earth system ensemble. *Global Change Biology*, doi:10.1111/gcb.13733 (2017).

11 Verbesselt, J. *et al.* Remotely sensed resilience of tropical forests. *Nature Climate Change* **6**, 1028-1031, doi:10.1038/nclimate3108 (2016).

12 Lenton, T. M. *et al.* Tipping elements in the Earth's climate system. *Proceedings of the National Academy of Sciences* **105**, 1786-1793, doi:10.1073/pnas.0705414105 (2008).

13 Dirzo, R. & Raven, P. H. Global State of Biodiversity and Loss. *Annual Review of Environment and Resources* **28**, 137-167, doi:10.1146/annurev.energy.28.050302.105532 (2003).

14 Malhi, Y. *et al.* Climate Change, Deforestation, and the Fate of the Amazon. *Science* **319**, 169-172, doi:10.1126/science.1146961 (2008).

15 Brienen, R. J. W. *et al.* Long-term decline of the Amazon carbon sink. *Nature* **519**, 344-348, doi:10.1038/nature14283 (2015).

16 Feldpausch, T. R. *et al.* Amazon forest response to repeated droughts. *Global Biogeochemical Cycles* **30**, 964-982, doi:10.1002/2015gb005133 (2016).

17 Hubau, W. *et al.* Asynchronous carbon sink saturation in African and Amazonian tropical forests. *Nature* **579**, 80-87, doi:10.1038/s41586-020-2035-0 (2020).

18 Boers, N., Marwan, N., Barbosa, H. M. J. & Kurths, J. A deforestation-induced tipping point for the South American monsoon system. *Scientific Reports* **7**, 41489, doi:10.1038/srep41489 (2017).

19 Brando, P. M. *et al.* Abrupt increases in Amazonian tree mortality due to drought-fire interactions. *Proceedings of the National Academy of Sciences* **111**, 6347-6352, doi:10.1073/pnas.1305499111 (2014).

20 Pueyo, S. *et al.* Testing for criticality in ecosystem dynamics: the case of Amazonian rainforest and savanna fire. *Ecology Letters* **13**, 793-802, doi:10.1111/j.1461-0248.2010.01497.x (2010).

21 Salati, E., Dall'Olio, A., Matsui, E. & Gat, J. R. Recycling of water in the Amazon Basin: An isotopic study. *Water Resources Research* **15**, 1250-1258, doi:10.1029/wr015i005p01250 (1979).

22 Jones, C., Lowe, J., Liddicoat, S. & Betts, R. Committed terrestrial ecosystem changes due to climate change. **2**, 484-487, doi:10.1038/ngeo555 (2009).

23 Friend, A. D., Stevens, A. K., Knox, R. G. & Cannell, M. G. R. A process-based, terrestrial biosphere model of ecosystem dynamics (Hybrid v3.0). *Ecological Modelling* **95**, 249-287, doi:10.1016/s0304-3800(96)00034-8 (1997).

24 Poulter, B. *et al.* Robust dynamics of Amazon dieback to climate change with perturbed ecosystem model parameters. *Global Change Biology*, doi:10.1111/j.1365-2486.2009.02157.x (2010).

25 Sitch, S. *et al.* Evaluation of the terrestrial carbon cycle, future plant geography and climate-carbon cycle feedbacks using five Dynamic Global Vegetation Models (DGVMs). *Global Change Biology* **14**, 2015-2039, doi:10.1111/j.1365-2486.2008.01626.x (2008).

26 Jones, C., Lowe, J., Liddicoat, S. & Betts, R. Committed terrestrial ecosystem changes due to climate change. *Nature Geoscience* **2**, 484-487, doi:10.1038/ngeo555 (2009).

27 Wissel, C. A universal law of the characteristic return time near thresholds. **65**, 101-107, doi:10.1007/bf00384470 (1984).
28 Scheffer, M. *et al.* Early-warning signals for critical transitions. *Nature* **461**, 53-59, doi:10.1038/nature08227 (2009).
29 Pimm, S. L. The complexity and stability of ecosystems. *Nature* **307**, 321-326, doi:10.1038/307321a0 (1984).
30 Dakos, V. *et al.* Slowing down as an early warning signal for abrupt climate change. *Proceedings of the National Academy of Sciences* **105**, 14308-14312, doi:10.1073/pnas.0802430105 (2008).
31 Held, H. & Kleinen, T. Detection of climate system bifurcations by degenerate fingerprinting. **31**, n/a-n/a, doi:10.1029/2004gl020972 (2004).
32 Boulton, C. A., Good, P. & Lenton, T. M. Early warning signals of simulated Amazon rainforest dieback. *Theor Ecol* **6**, 373-384, doi:10.1007/s12080-013-0191-7 (2013).
33 Lenton, T. M. Early warning of climate tipping points. *Nature Climate Change* **1**, 201-209, doi:10.1038/nclimate1143 (2011).
34 Biggs, R., Carpenter, S. R. & Brock, W. A. Turning back from the brink: Detecting an impending regime shift in time to avert it. *Proceedings of the National Academy of Sciences* **106**, 826-831, doi:10.1073/pnas.0811729106 (2009).
35 Moesinger, L. *et al.* The global long-term microwave Vegetation Optical Depth Climate Archive (VODCA). *Earth System Science Data* **12**, 177-196, doi:10.5194/essd-12-177-2020 (2020).
36 Vermote, E., NOAA CDR Program. NOAA Climate Data Record (CDR) of AVHRR Normalized Difference Vegetation Index (NDVI), Version 5. Accessed 2021-02-10. NOAA National Centers for Environmental Information. doi:10.7289/V5ZG6QH9 (2019).
37 Liu, Y. Y. *et al.* Recent reversal in loss of global terrestrial biomass. *Nature Climate Change* **5**, 470-474, doi:10.1038/nclimate2581 (2015).
38 Myneni, R. B., Keeling, C. D., Tucker, C. J., Asrar, G. & Nemani, R. R. Increased plant growth in the northern high latitudes from 1981 to 1991. *Nature* **386**, 698-702, doi:10.1038/386698a0 (1997).
39 Friedl, M. & Sulla-Menashe, D. MCD12C1 MODIS/Terra+Aqua Land Cover Type Yearly L3 Global 0.05Deg CMG V006. NASA EOSDIS Land Processes DAAC. Accessed 2020-04-20. doi:10.5067/MODIS/MCD12C1.006 (2015).
40 Funk, C. *et al.* The climate hazards infrared precipitation with stations—a new environmental record for monitoring extremes. *Scientific Data* **2**, 150066, doi:10.1038/sdata.2015.66 (2015).
41 Ciemer, C. *et al.* Higher resilience to climatic disturbances in tropical vegetation exposed to more variable rainfall. *Nature Geoscience* **12**, 174-179, doi:10.1038/s41561-019-0312-z (2019).
42 Wuyts, B., Champneys, A. R. & House, J. I. Amazonian forest-savanna bistability and human impact. *Nature Communications* **8**, doi:10.1038/ncomms15519 (2017).
43 Hirota, M., Holmgren, M., Van Nes, E. H. & Scheffer, M. Global Resilience of Tropical Forest and Savanna to Critical Transitions. *Science* **334**, 232-235, doi:10.1126/science.1210657 (2011).
44 Tian, F. *et al.* Remote sensing of vegetation dynamics in drylands: Evaluating vegetation optical depth (VOD) using AVHRR NDVI and in situ green biomass data over West African Sahel. *Remote Sensing of Environment* **177**, 265-276, doi:10.1016/j.rse.2016.02.056 (2016).
45 Marengo, J. A. *et al.* Changes in Climate and Land Use Over the Amazon Region: Current and Future Variability and Trends. *Frontiers in Earth Science* **6**, doi:10.3389/feart.2018.00228 (2018).
46 Leite-Filho, A. T., Costa, M. H. & Fu, R. The southern Amazon rainy season: The role of deforestation and its interactions with large-scale mechanisms. *International Journal of Climatology*, doi:10.1002/joc.6335 (2019).

47 Dakos, V., Van Nes, E. H., D'Odorico, P. & Scheffer, M. Robustness of variance and autocorrelation as indicators of critical slowing down. *Ecology* **93**, 264-271, doi:10.1890/11-0889.1 (2012).
48 Cleveland, R. B., Cleveland, W. S. & Terpenning, I. STL: A Seasonal-Trend Decomposition Procedure Based on Loess. *Journal of Official Statistics* **6**, 3 (1990).
49 Rypdal, M. Early-Warning Signals for the Onsets of Greenland Interstadials and the Younger Dryas–Preboreal Transition. *Journal of Climate* **29**, 4047-4056, doi:10.1175/jcli-d-15-0828.1 (2016).
50 Boers, N. Early-warning signals for Dansgaard-Oeschger events in a high-resolution ice core record. *Nature Communications* **9**, doi:10.1038/s41467-018-04881-7 (2018).

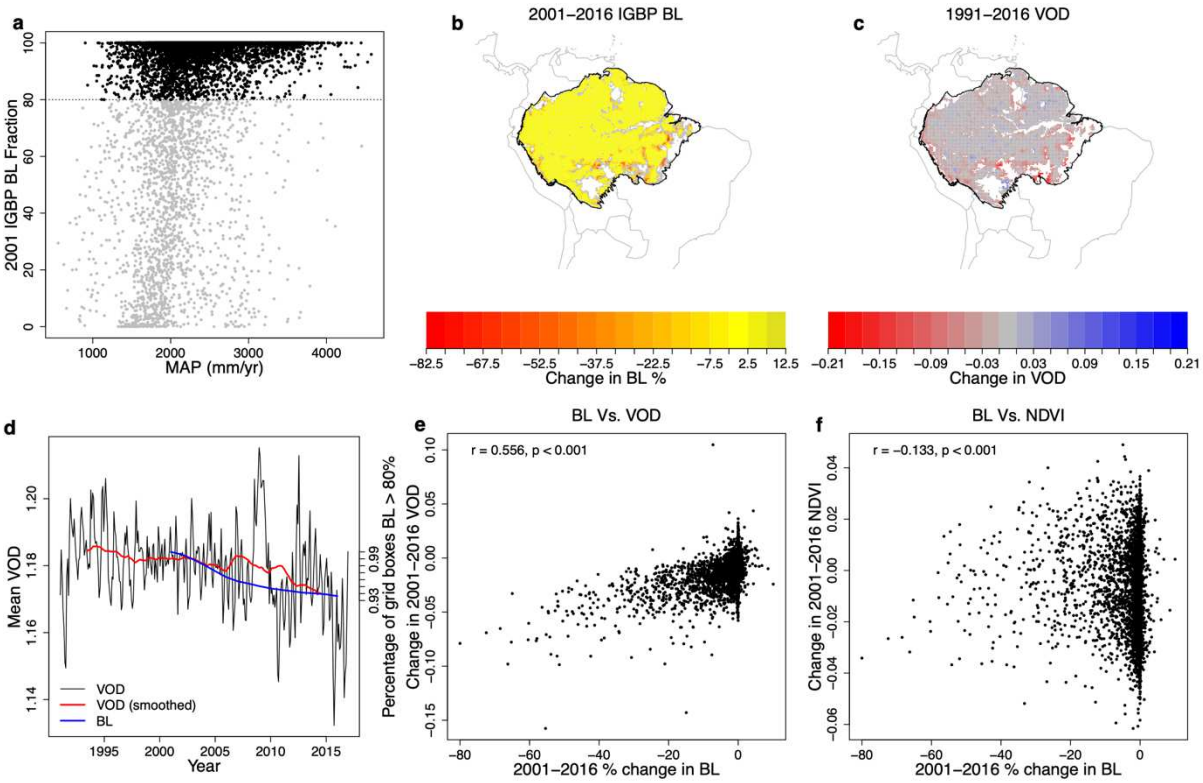

Figure 1: Relationships between different vegetation and rainfall data for the Amazon basin. (a) The relationship between 2001-2016 mean annual precipitation (MAP) from CHIRPS[40] and 2001 MODIS Land Cover Evergreen Broadleaf (BL) fraction[39]. Points coloured black are where 2001 BL >= 80%. (b) Change in the BL fraction from 2001 to 2016 for grid points where BL > 80% in 2001. Points that are predominantly BL in 2001 according to the MODIS 2001 dataset, but <80% are shown in grey. (c,d) Change in Vegetation Optical Depth (VOD) Climate Archive Ku-Band product[35] from 1991-2016 (difference between the 2012-2016 and 1991-1995 means) for the grid points where BL > 80% in 2001, along with the median time series in these points. Also shown in blue on (d) is the annual percentage of grid boxes that have BL > 80%, from those that have BL > 80% in 2001. Sharp decreases in BL fraction and VOD could be directly attributed to deforestation. In these cases of externally forced forest loss, we may not see changes in AR(1) unless there was an underlying loss of resilience beforehand.

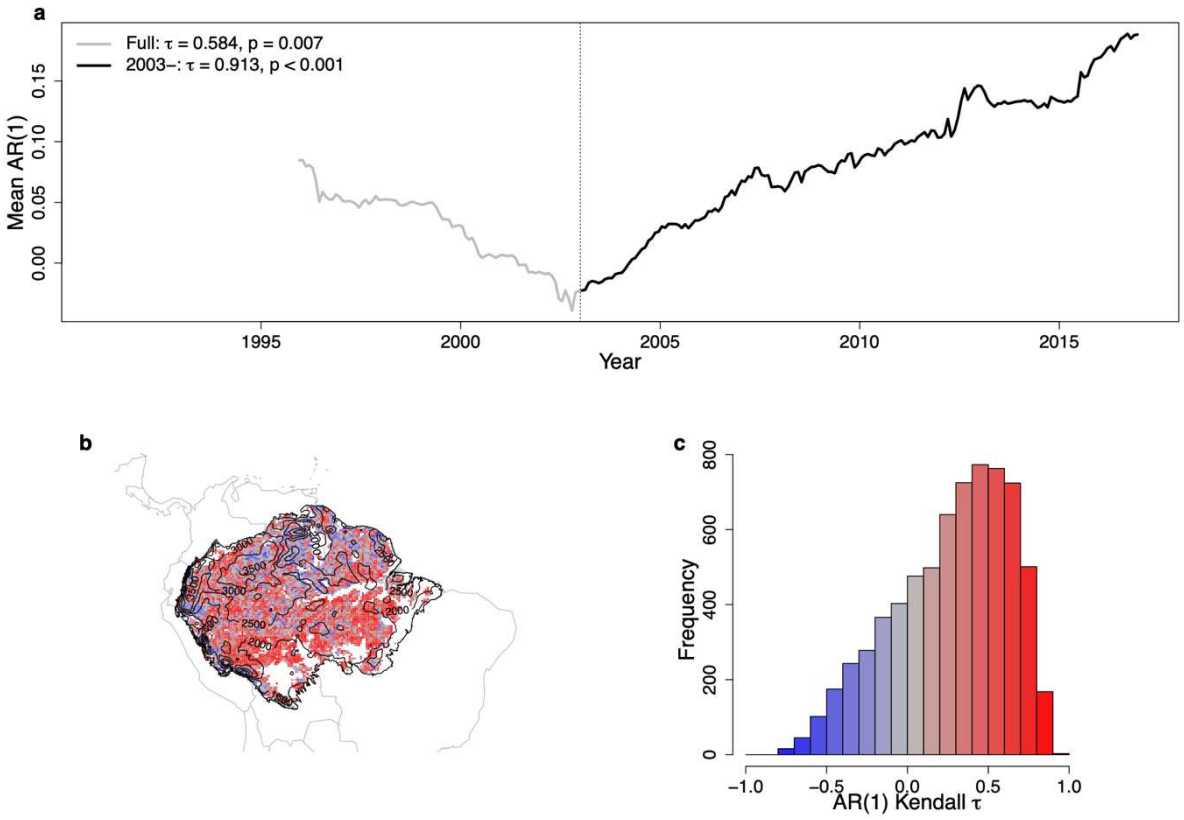

328

329 **Figure 2: Changes in Amazon vegetation resilience since the early 1990s and from**
330 **2003.** (a) Mean VOD AR(1) time series created from grid points that have >= 80% BL
331 fraction in the Amazon basin. The full AR(1) time series from 1991 (grey) has a Kendall τ
332 value of 0.584 ($p = 0.007$) and from 2003 (black), a value of 0.913 ($p < 0.001$). (b) A map of
333 the Kendall τ values of individual grid boxes from 2003, shown alongside contours of MAP
334 (mm/year) over the same time period. (c) A histogram of the Kendall τ values from the map.

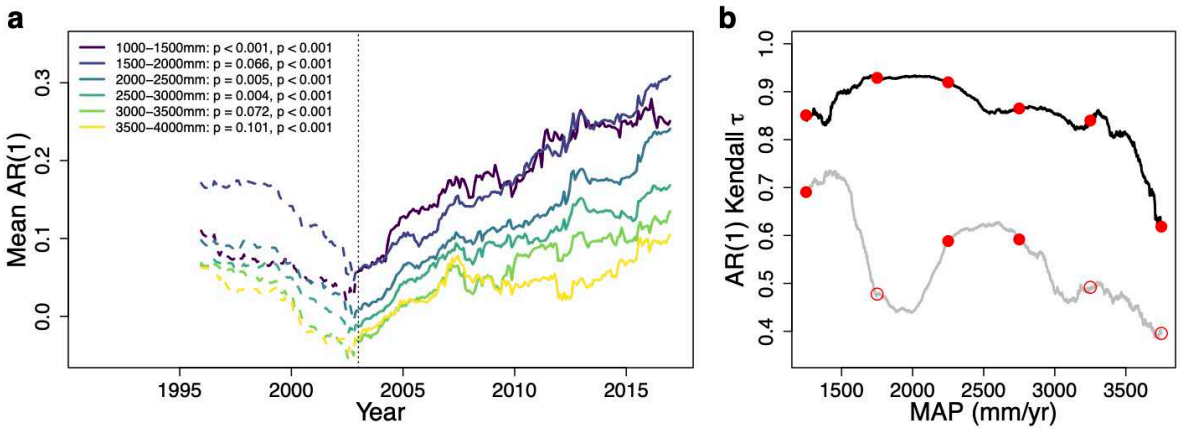

335

336 **Figure 3: The relationship between annual rainfall sums and vegetation resilience.** (a)
337 Example VOD AR(1) time series for 500mm MAP-bands from 1991 (dotted lines) and from
338 2003 (solid lines). (b) Full VOD AR(1) Kendall τ series for a sliding MAP-band, from 1991
339 (grey) and from 2003 (black). Red circles show the results from panel (a) and are closed if
340 the Kendall τ value is significantly positive ($p < 0.05$) and open otherwise. The tendency of
341 the relationships in (b) are $\tau = -0.423$ (grey) and $\tau = -0.553$ (black), confirming there is a
342 more severe decrease in resilience with lower rainfall values.

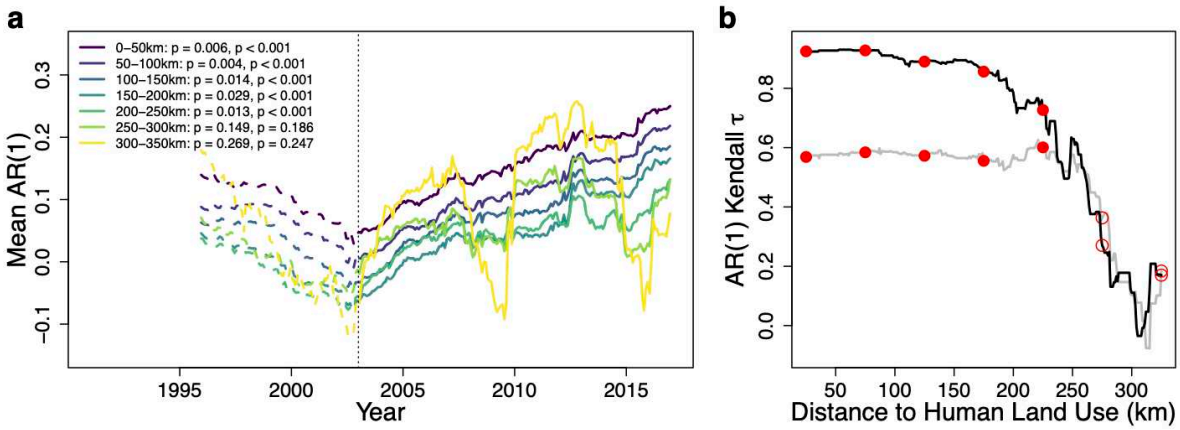

Figure 4: The relationship between human activity and vegetation resilience. (a) Example VOD AR(1) time series for 25km bands measuring the distance a forested grid box is from a human land use grid box (defined in the Methods from the MODIS Land Cover product[39] and shown in Supplementary Fig. 6), from 1991 (dotted lines) and from 2003 (solid lines). (b) Full VOD AR(1) Kendall τ series for a sliding distance-band, from 1991 (grey) and from 2003 (black). Red circles show the results from panel (a) and are closed if the Kendall τ value is significantly positive ($p < 0.05$) and open otherwise. The tendency of these relationships are $\tau = -0.553$ (grey) and $\tau = -0.857$ (black), showing there is a more severe decrease in resilience with increasing proximity to human land use.

353 **Methods**

354 **Datasets.** We use the Amazon basin
355 (http://worldmap.harvard.edu/data/geonode:amapoly_ivb) as our region of study. The main
356 dataset used to determine forest health is from the Vegetation Optical Depth Climate Archive
357 (VODCA)[35], of which we use the Ku-band product. This data is available at 0.25°x0.25° at a
358 monthly resolution from January 1988 to December 2016. We also use NOAA AVHRR
359 NDVI[36]. For precipitation data, we use the CHIRPS dataset[40] downloaded from Google Earth
360 Engine (GEE) at a monthly resolution. Finally, to determine land cover types, we used the
361 IGBP MODIS land cover dataset MCD12C1[39]. All of these datasets are at a higher spatial
362 resolution than the VODCA dataset and thus we linearly interpolate them to match the lower
363 resolution.

364 For the vegetation datasets that we measure the resilience indicators on (see below), we
365 use STL decomposition[48] using the stl() function in R. This splits time series in each grid box
366 into an overall trend, a repeating annual cycle (by using the 'periodic' option for the seasonal
367 window), and a residual component. We use the residual component in our resilience
368 analysis. Finding the first 3 years had large jumps in VOD which were seen when testing
369 other regions of the world as well as in the Amazon region, we restrict our analysis to
370 January 1991 to December 2016.

371 To test the robustness of the detrending, we also vary the size of the trend window in the
372 stl() function. The results from these alternatively detrended time series are shown
373 Supplementary Figure 2.

374 **Grid box selection.** We use the IGBP MODIS land cover dataset at the resolution described
375 above to determine which grid boxes to use in our analysis. The dataset is at an annual
376 resolution from 2001 to 2018 (but we only use the time series up to 2016 to match the time
377 span of our VOD and NDVI datasets). To focus on changes in forest resilience, we use grid
378 boxes where the evergreen broadleaf fraction is greater than or equal to 80% in 2001. Grid

boxes are treated as human land use area if the built-up, croplands, or vegetation mosaics fraction is greater than 0% in 2016. to We believe using these years to determine these factors is the most cautious and least biased way to choose which grid boxes to use.

We measure the minimum distance between forested Amazon basin grid boxes and human land use grid boxes using the latitude and longitude of each grid point. We do not restrict human land use grid boxes to the Amazon basin region when determining the forested grid boxes distance from them. This ensures that human land use grid boxes just outside the region which could be the closest, are not ignored.

To ensure that the pattern of changes in resilience is not a consequence of more settlements being in the south east of the region combined with the gradient of rainfall from northwest to southeast typical of the rainforest, we measure the correlation between MAP and the distances from the urban grid boxes. Although this is statistically significant, it is relatively weak (Spearman's ρ=0.109, p<0.001) and as such we are confident that there are separate processes that causes these relationships.

Resilience indicator AR(1). We measure our resilience indicator on the residual component of the decomposed vegetation time series. We focus on lag-1 autocorrelation (AR(1)), which provides the most robust indicator for critical slowing down prior to bifurcation-induced transitions and has been widely used for this purpose[11,28,30]. We measure it on a sliding window length equal to 5 years (60 months). The sliding window creates a time series of the AR(1) coefficient in each location.

From linearization and the analogy to the Ornstein-Uhlenbeck process, it holds approximately that for discrete time steps of width Δt (one month in the case at hand):

$$AR(1) = e^{-\kappa \Delta t},$$

where κ is the linear recovery rate. A decreasing recovery rate κ implies that the system's capability to recover from perturbations is progressively lost, corresponding to diminishing

stability or resilience of the attained equilibrium state. From the above equation it is clear that the AR(1) increases with decreasing κ. The point at which stability is lost and the system will undergo a critical transition to shift to a new equilibrium state, corresponds to $\kappa = 0$ and AR(1) = 1, respectively.

Measuring AR(1) across the whole time series provides information about the characteristic timescales of the two vegetation datasets we use[31]. Inverting κ gives the characteristic time scale of the system; for the VOD, we find $1/\kappa = 1.240$ months, whereas for the NDVI, we find $1/\kappa = 0.838$ months when using the mean AR(1) value across the region. This suggests that, in accordance with our interpretation of the two satellite-derived variables, the NDVI is more sensitive to shorter-term vegetation changes such as leaf greenness, while the VOD's Ku band is sensitive to longer-term changes such as variability in the thickness of forest stems.

Creation and tendency of AR(1) and variance time series. For analysis where either MAP- or distance-bands are used to create an AR(1) or variance series, we calculate the mean AR(1) or variance value in each month for forested Amazon basin grid boxes, from which the tendency of this mean series can be calculated. Alternatively, the Kendall τ for each band can be calculated by taking the mean Kendall τ for each individual grid box that is within the band. Results from this method are shown in Supplementary Figure 10 for AR(1).

The tendency of the indicator is determined in terms of Kendall's τ. This is a rank correlation coefficient with one variable taken to be time. Kendall's tau values of 1 imply that the time series is always increasing, -1 always decreasing, and 0 no overall trend. Following previous work[30,49,50], we test the statistical significance of positive tendencies using a test based on phase surrogates that preserve both the variance and the serial correlations of the time series from which the surrogates are constructed. Specifically, we compute the Fourier transform of each time series for which we want to the significance of Kendal's τ, then randomly permute the phases and finally apply in inverse Fourier transform. Since this preserves the power spectral density, it also preserves the autocorrelation function due to

the Wiener-Khinchin theorem. For each time series this procedure is repeated 100,000 times to obtain the surrogates. Kendall's τ is computed for each surrogate to obtain the null model distribution (corresponding to the assumption of the same variance and autocorrelation but no underlying trend), from which the significance thresholds are computed as the 95^{th} percentiles.

Data and code availability

Data is available from the sources listed. R code is available on request.

Methods references

48 Cleveland, R. B., Cleveland, W. S. & Terpenning, I. STL: A Seasonal-Trend Decomposition Procedure Based on Loess. *Journal of Official Statistics* **6**, 3 (1990).

49 Rypdal, M. Early-Warning Signals for the Onsets of Greenland Interstadials and the Younger Dryas–Preboreal Transition. *Journal of Climate* **29**, 4047-4056, doi:10.1175/jcli-d-15-0828.1 (2016).

50 Boers, N. Early-warning signals for Dansgaard-Oeschger events in a high-resolution ice core record. *Nature Communications* **9**, doi:10.1038/s41467-018-04881-7 (2018).

Acknowledgements. NB acknowledges funding by the Volskwagen foundation. This is TiPES contribution #X. The TiPES project ('Tipping Points in the Earth System') has received funding from the European Union's Horizon 2020 research and innovation programme under grant agreement No. 820970. CAB and TML were supported by the Leverhulme Trust (RPG-2018-046). TML was also supported by a Turing Fellowship.

Author contributions. NB and CAB conceived and designed the study with input from TML. CAB performed the numerical analysis with contributions from NB. All authors discussed results and drew conclusions. CAB wrote the paper with contributions from NB and TML.

Competing interests. The authors declare no competing interests.

Additional Information

Supplementary Information accompanies the paper.

Correspondence should be addressed to CAB (c.a.boulton@exeter.ac.uk)

Figures

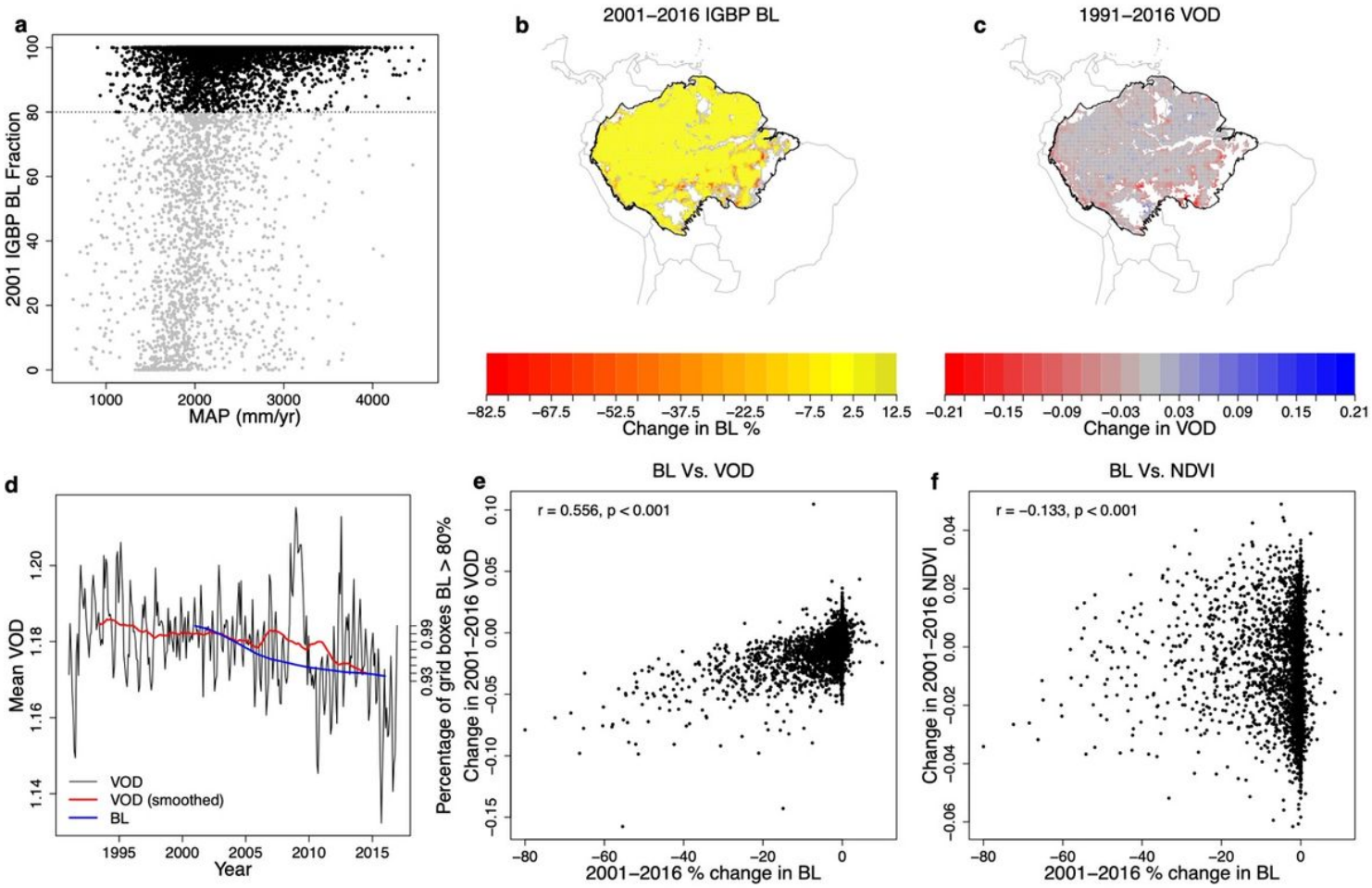

Figure 1

Relationships between different vegetation and rainfall data for the Amazon basin. (a) The relationship between 2001-2016 mean annual precipitation (MAP) fro CHIRPS40 and 2001 MODIS Land Cover Evergreen Broadleaf (BL) fraction39. Pointcoloured black are where 2001 BL >= 80%. (b) Change in the BL fraction from 2001 to 2016 for grid points where BL > 80% in 2001. Points that are predominantly BL in 2001 according to the MODIS 2001 dataset, but <80% are shown in grey. (c,d) Change in Vegetation Optical Depth (VOD) Climate Archive Ku-Band product35 from 1991-2016 (difference between the 2012-2016 and 1991-1995 means) for the grid points where BL > 80% in 2001, along with the median time series in these points. Also shown in blue on (d) is the annual percentage of grid boxes that have BL > 80%, from those that have BL > 80% in 2001. Sharp decreases in BL fraction and VOD could be directly attributed to deforestation. In these cases of externally forced forest loss, we may not see changes in AR(1) unless there was an underlying loss of resilience beforehand.

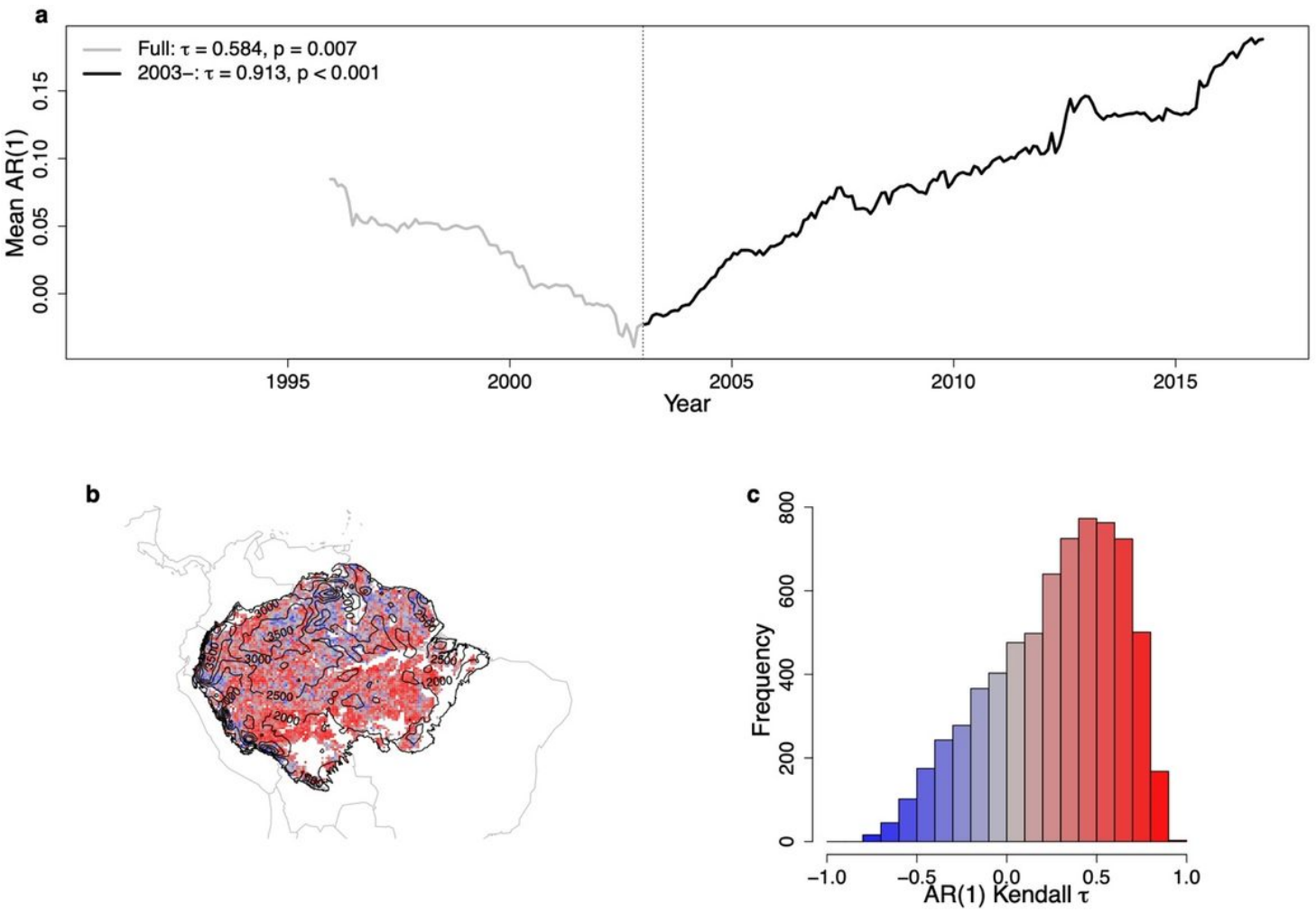

Figure 2

Changes in Amazon vegetation resilience since the early 1990s and from 2003. (a) Mean VOD AR(1) time series created from grid points that have >= 80% BL fraction in the Amazon basin. The full AR(1) time series from 1991 (grey) has a Kendall t value of 0.584 (p = 0.007) and from 2003 (black), a value of 0.913 (p < 0.001). (b) A map of the Kendall t values of individual grid boxes from 2003, shown alongside contours of MAP (mm/year) over the same time period. (c) A histogram of the Kendall t values from the map.

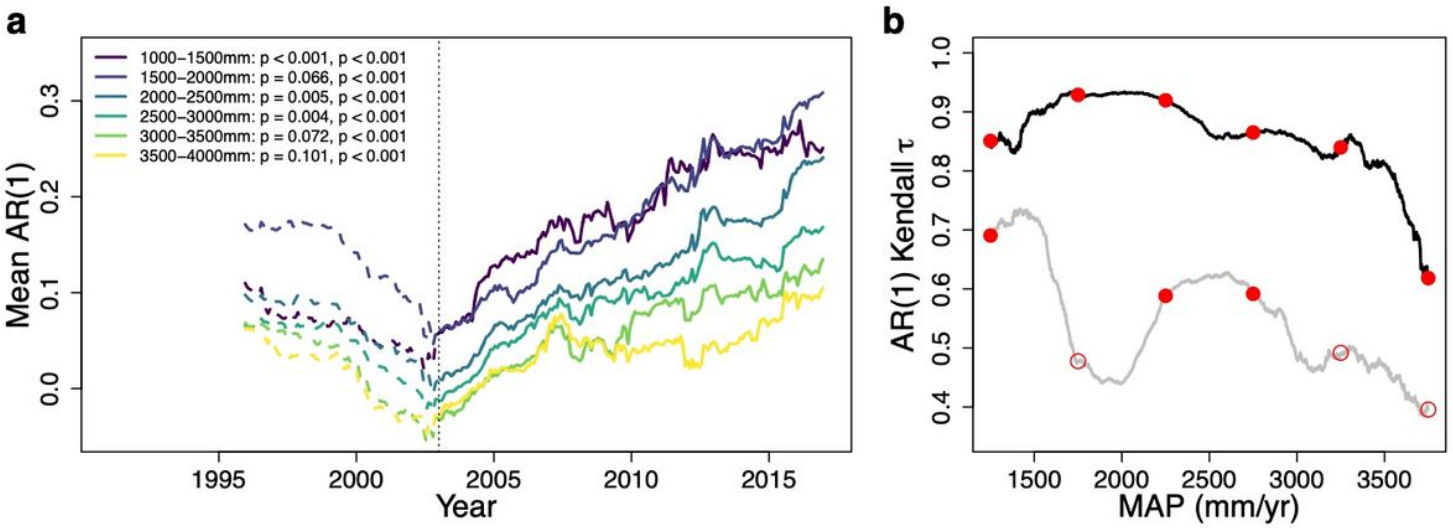

Figure 3

The relationship between annual rainfall sums and vegetation resilience. (a) Example VOD AR(1) time series for 500mm MAP-bands from 1991 (dotted lines) and from 2003 (solid lines). (b) Full VOD AR(1) Kendall t series for a sliding MAP-band, from 1991 (grey) and from 2003 (black). Red circles show the results from panel (a) and are closed if the Kendall t value is significantly positive ($p < 0.05$) and open otherwise. The tendency of the relationships in (b) are t = -0.423 (grey) and t = -0.553 (black), confirming there is a more severe decrease in resilience with lower rainfall values.

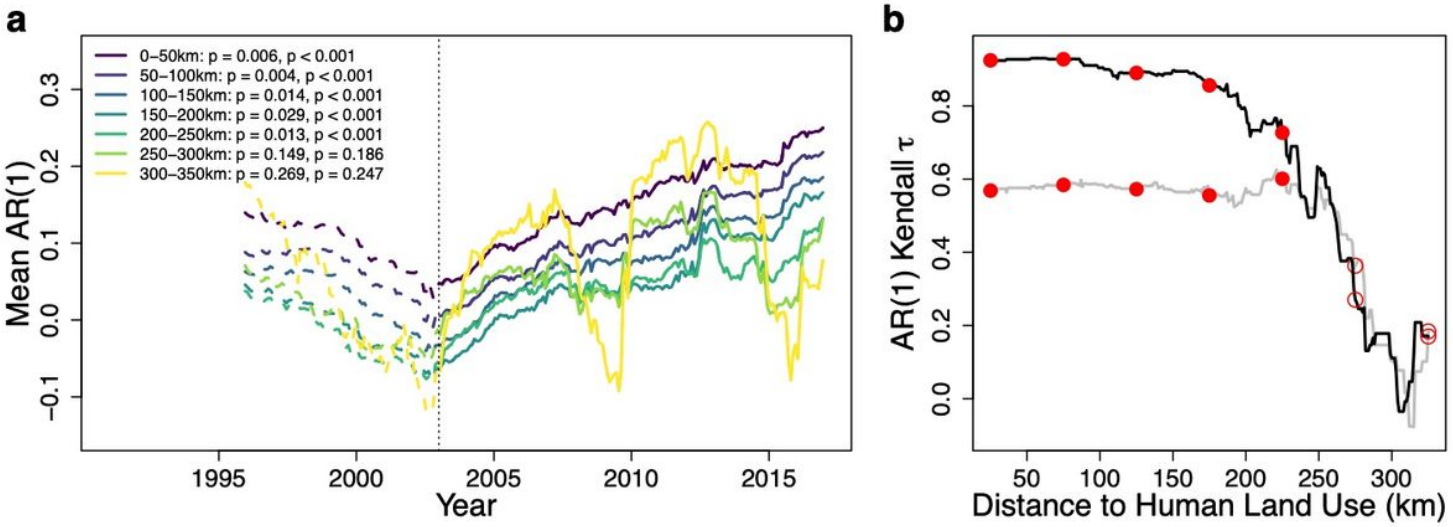

Figure 4

The relationship between human activity and vegetation resilience. (a) Example VOD AR(1) time series for 25km bands measuring the distance a forested grid box is from a human land use grid box (defined in the Methods from the MODIS Land Cover product39 and shown in Supplementary Fig. 6), from 1991 (dotted lines) and from 2003 (solid lines). (b) Full VOD AR(1) Kendall t series for a sliding distance-band,

from 1991 (grey) and from 2003 (black). Red circles show the results from panel (a) and are closed if the Kendall t value is significantly positive ($p < 0.05$) and open otherwise. The tendency of these relationships are $t = -0.553$ (grey) and $t = -0.857$ (black), showing there is a more severe decrease in resilience with increasing proximity to human land use.

Supplementary Files

This is a list of supplementary files associated with this preprint. Click to download.

- SupplementaryInfo.pdf